ACS APPLIED MATERIALS & INTERFACES

www.acsami.org

Research Article

DNA Hydrogel-Based Three-Dimensional Electron Transporter and Its Application in Electrochemical Biosensing

Xiaoxia Mao, Dongsheng Mao, Tianshu Chen, Mohammed Jalalah, Mohammed S. Al-Assiri, Farid A. Harraz,* Xiaoli Zhu,* and Genxi Li

Cite This: *ACS Appl. Mater. Interfaces* 2020, 12, 36851−36859

Read Online

ACCESS | Metrics & More | Article Recommendations | Supporting Information

ABSTRACT: Electrochemical biosensing relies on electron transport on the electrode surface. However, the limited functional area of the two-dimensional electrode prevents the qualitative breakthrough in the efficiency of electron transfer. Here, a three-dimensional electron transporter was constructed to improve the efficiency of electron transfer by using an interface-immobilized DNA hydrogel. A three-dimensional pure DNA hydrogel is constructed and used as a scaffold for electron transfer. Then, an electron mediator is embedded in the DNA hydrogel through intercalative binding, and DNAzyme with intrinsic peroxidase-like activity is introduced at the node of the hydrogel scaffold to fabricate an electrochemical biosensor. The conduction of the electron mediator in the scaffold enables the acquisition of long-distance DNAzyme catalytic signals, thereby overcoming the limitation of two-dimensional electrodes. This three-dimensional electron transporter is significant for enriching the toolbox of electrochemical biosensing and can provide potential support for the development of highly sensitive biosensors.

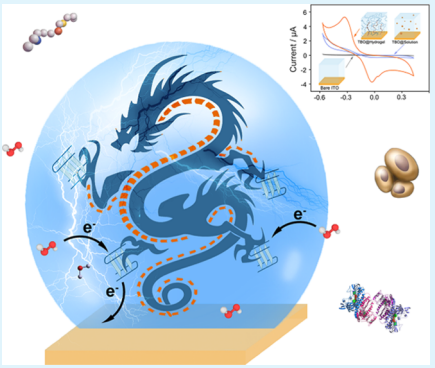

KEYWORDS: *electron transfer, electrochemical, three-dimensional electron transporter, pure DNA hydrogel, biosensor*

1. INTRODUCTION

Electrochemical biosensing is an important part of modern analytical chemistry.[1,2] The most critical issue of electrochemical biosensing that is widely concerned is the functionalization of the working electrode[3] because molecular recognition, signal conversion, and signal acquisition are all conducted at the electrode/electrolyte interface.[4,5] However, the two-dimensional electrode (solid)/electrolyte (liquid) interface imposes great limitations on many aspects of electrochemical biosensing.[6,7] Taking molecular recognition for instance, the molecular interaction efficiency at the solid/liquid interface is much lower than that in a liquid system, which will result in the requirement of a long equilibration time.[8] To address this problem, some researchers consider placing molecular recognition in liquid and then transferring it to the electrode surface through a more efficient linker or chemical reaction (e.g. click chemistry) so as to improve the molecular interaction efficiency.[9,10] For signal acquisition, the signal intensity is usually unsatisfactory because the limited geometric area of the electrode only allows a few number of active signal molecules to transfer electrons with the electrode.[11] The most common strategy to solve this problem is to increase the specific surface area of the electrode surface by using nanomaterials with good conductivity (e.g. gold nanoparticles, graphene, and carbon nanotubes) to functionalize the electrode.[12−14] An alternative approach is to construct a multilayer electron transporter through a layer-by-layer strategy.[15] Nevertheless, limitations still exist: the former does not fundamentally overcome the limitation of the two-dimensional interface, while the latter is tedious to operate.[16,17]

The DNA hydrogel is a three-dimensional network composed of DNA through Watson−Crick base pairing or random coiling.[18,19] Thanks to its special properties such as swelling, shape recovery, responsiveness, and encapsulation, it has been successfully applied in different kinds of biosensors.[20−23] Also, considering the advantage that the three-dimensional network of the DNA hydrogel can be formed through one-pot assembly and the fact that the DNA biosensor and aptasensor have been widely developed and applied,[24,25] it will be of great significance for the development of higher-performance electrochemical biosensors if the DNA hydrogel can be adopted to a functionalized electrode and work as a scaffold to construct a three-dimensional electron transporter. To achieve this concept, there are three major challenges: (1) reagents such as analytes should be allowed to enter the hydrogel to meet the needs of electrochemical analysis. In our previous work, we constructed a DNA hydrogel, which

Received: May 2, 2020
Accepted: July 14, 2020
Published: July 14, 2020

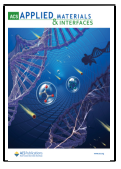

https://dx.doi.org/10.1021/acsami.0c08064
ACS Appl. Mater. Interfaces 2020, 12, 36851−36859

Table 1. Sequences of Oligonucleotides Used in This Work

name	sequence (5′−3′)	modification
circular DNA 1	TAGATTTTTTTTTTTTTTTAGGGTTAGGG TTTTTTTTTTTTTTAGGGTTAGGGTTTT ATGTGG	cyclization
circular DNA 2	TAGATTTTTTTTTTTTTTTAGACTTACAGTTTTTTTTTTTTTTAGACTTACAGTTTTATGTGG	cyclization
primer 1	ACTCTTAGTTATCTA CCACAT	5′-NH_3
primer 2	TTT TTT TTT TTT	
G-quadruplex	GGGTTAGGGTTAGGGTTAGGG	

partially addressed this issue by satisfying the free diffusion of small molecules.[26] (2) The DNA hydrogel should be immobilized on the electrode surface. This challenge has also been addressed before.[27] (3) A strategy to transfer electrons in the three-dimensional DNA hydrogel should be explored because DNA itself is not conductive. This issue remains to be solved, which restricts the implementation of the DNA hydrogel-based three-dimensional electron transporter.

In this work, we conquered the last challenge, constructed a DNA hydrogel-based three-dimensional electron transporter and thereby fabricated a high-performance electrochemical biosensor. Our strategy is to intercalate electron mediators in the scaffold of the DNA hydrogel through self-assembly. The repeated base-pairing of the double helix structure of DNA in nanoscale allows the electron hopping among the intercalated electron mediators, making electron transport through the three-dimensional network possible. In addition to the electron mediators, G-quadruplex/hemin DNAzyme with intrinsic peroxidase-like activity is also introduced at the node of the DNA hydrogel scaffold so as to fabricate an electrochemical biosensor. Based on this architecture, the acquisition of long-distance DNAzyme catalytic signals and high-performance electrochemical biosensing can be achieved. This three-dimensional electron transporter tackles the above three challenges, thus enriching the toolbox of electrochemical biosensing and providing potential support for the development of highly sensitive biosensors.

2. EXPERIMENTAL SECTION

2.1. Materials. All oligonucleotides used in this work were synthesized and purified by TaKaRa Biotechnology Co. Their sequences are listed in Table 1. phi29 DNA polymerase was purchased from New England Biolabs Inc. Hemin (from bovine), tris(2-carboxyethyl)phosphine, and 3-(aminopropyl)triethoxysilane (APTES) were obtained from Sigma-Aldrich. 2,2′-Azino-bis(3-ethylbenzothiazoline-6-sulfonic acid) was obtained from Sangon Biotech. SYBR Green I was purchased from Shanghai YuanYe Biotechnology Co., Ltd. Hydrogen peroxide (H_2O_2) and toluidine blue O (TBO) were purchased from Sinopharm Chemical Reagent Co., Ltd. All reagents were of analytical grade and used as received without further purification. HL60 cells were supplied by Shanghai GeneChem Co., Ltd. DAPI and Cy3 were obtained from LiTTLE-PA Sciences Co., Ltd. Cy3-labeled goat antirabbit IgG secondary antibodies (Cy3-IgG) were obtained from Thermo Fisher Scientific Inc. Water used throughout this work was purified by the Milli-Q system (18.2 MΩ·cm^{-1}).

All isothermal amplifications were performed in an Eppendorf Mastercycler (Hamburg, Germany). A thermostat cultivating shaker (Eppendorf, Germany) was used to provide a constant temperature and rotation speed in the experiment. The elemental distributions of the DNA hydrogel-based three-dimensional electron transporter were characterized by JOEL scanning electron microscopy (SEM) JSM-6301/Oxford Link-300 energy dispersive spectrum (SEM/EDS) elemental mapping (U = 20 kV). The morphology of the DNA hydrogel-based three-dimensional electron transporter was observed by scanning electron microscopy (Carl Zeiss Inc., Germany) (U = 5 kV). SEM samples were dried in a vacuum oven for 8 h and coated with Au for further measurement. Transmission electron microscopy (TEM) of the DNA hydrogel was performed using a JEOL-2100 transmission electron microscope (JEOL, Japan) (U = 200 kV). The Young's modulus measurement of the DNA hydrogel was conducted using atom force microscopy (AFM, Agilent 5500 AFM system, Agilent Technologies, USA) under contact mode. An approach and retract speed of the AFM probe of 2 μM·s^{-1} was used with a trigger force of 1 nN, and the Young's modulus was calculated by AFM using the Hertz model. Electrochemical experiments were carried out with an electrochemical analyzer (CH Instruments, model 660B). Confocal laser scanning microscopy images were snapped with a Leica LSM710 confocal laser scanning microscope (Leica Microsystems, Occult International Ltd., Germany).

2.2. Fabrication of the DNA Hydrogel-Based Three-Dimensional Electron Transporter. Indium-tin oxide (ITO) electrodes were used to support the DNA hydrogel-based three-dimensional electron transporter. The hydroxyl group on the electrode was first activated by sonicating the electrode in acetone, ethanol, and water for 20 min, respectively. Then, the electrode was incubated with freshly prepared 5% APTES (in ethanol) at 4 °C overnight. After APTES treatment, the electrode was immersed in anhydrous ethanol and then heated in water at 80 °C for 10 min to remove excess APTES. Next, the electrode was incubated with glutaraldehyde at 37 °C for 2 h, followed by washing with water and PBS buffer, respectively. Finally, the electrode was incubated with 5′-amino-modified primer 1 (5 μM) in PBS buffer for 2 h at 37 °C. Thus, a DNA primer-functionalized electrode was prepared.

The DNA hydrogel was fabricated as follows: First, 5 μM circular DNA working as the template, 50 mM dNTPs, and 1 unit/μL phi29 DNA polymerase were incubated with the as-prepared electrode at 30 °C for 4 h to initiate linear rolling circle amplification (LRCA) on the electrode surface. Then, 5 μM primer 2 was added and incubated at 30 °C for 6 h to launch hyperbranched rolling circle amplification (HRCA). A large amount of HRCA product on the surface of the electrode was further heated at 65 °C for 15 min to terminate the reaction and then cooled down to room temperature to form the three-dimensional DNA hydrogel. Finally, the as-prepared DNA hydrogel was successively incubated with 20 μM hemin for 2 h and 2 mM TBO for another 1 h. As a result, the DNA hydrogel-based three-dimensional electron transporter was fabricated on the surface of the ITO electrode. Before electrochemical analysis, the electrode was gently rinsed with PBS buffer (50 mM phosphate and 100 mM NaCl, pH 6.5) to remove nonspecifically adsorbed TBO. Some critical experimental conditions in the above experimental processes were obtained through systematic optimization, including the reaction time of LRCA (Figure S1), the concentration (Figure S2), and the incubation time (Figure S3) of hemin.

2.3. Electrochemical Measurements. Electrochemical measurements were carried out using a conventional three-electrode system with the DNA hydrogel-functionalized ITO electrode, a saturated calomel electrode, and a platinum plate as the working, reference, and counter electrodes, respectively. Cyclic voltammetric (CV) measurement was performed in PBS buffer (50 mM phosphate and 100 mM NaCl) with a scan rate of 20 mV·s^{-1}. The pH of the electrolyte was optimized to be 6.5 (Figure S4).

2.4. Study on the Anti-interference Ability of the Three-Dimensional Electron Transporter. First, the DNA hydrogel was stained with 10× SYBR Green I for 10 min at room temperature, followed by washing with 1× PBS. Subsequently, 20 μM Cy3, 20 μM Cy3-labeled IgG, or 1 × 10^5 cells/mL DAPI-stained cells was added

https://dx.doi.org/10.1021/acsami.0c08064
ACS Appl. Mater. Interfaces 2020, 12, 36851−36859

Scheme 1. Schematic Illustration of the DNA Hydrogel-Based Three-Dimensional Electron Transporter; (a) Schematic Illustration of the Fabrication of the Three-Dimensional Electron Transporter on the Surface of the ITO Electrode through HRCA; (b) Schematic Illustration of the Catalysis and Electron Transport in the Three-Dimensional Electron Transporter (Model (i), the DNAzyme is Incorporated at the Node of the Hydrogel Scaffold); (c) Molecular Docking Result of TBO and Double-Stranded DNA Obtained by Discovery Studio 2018; Schematic Illustration of the Catalysis and Electron Transport in (d) (Model (ii); (a) Separate DNAzyme is Put in the Electrolyte) and (e) (Model (iii) the Separate DNAzyme is Encapsulated in the DNA Hydrogel)

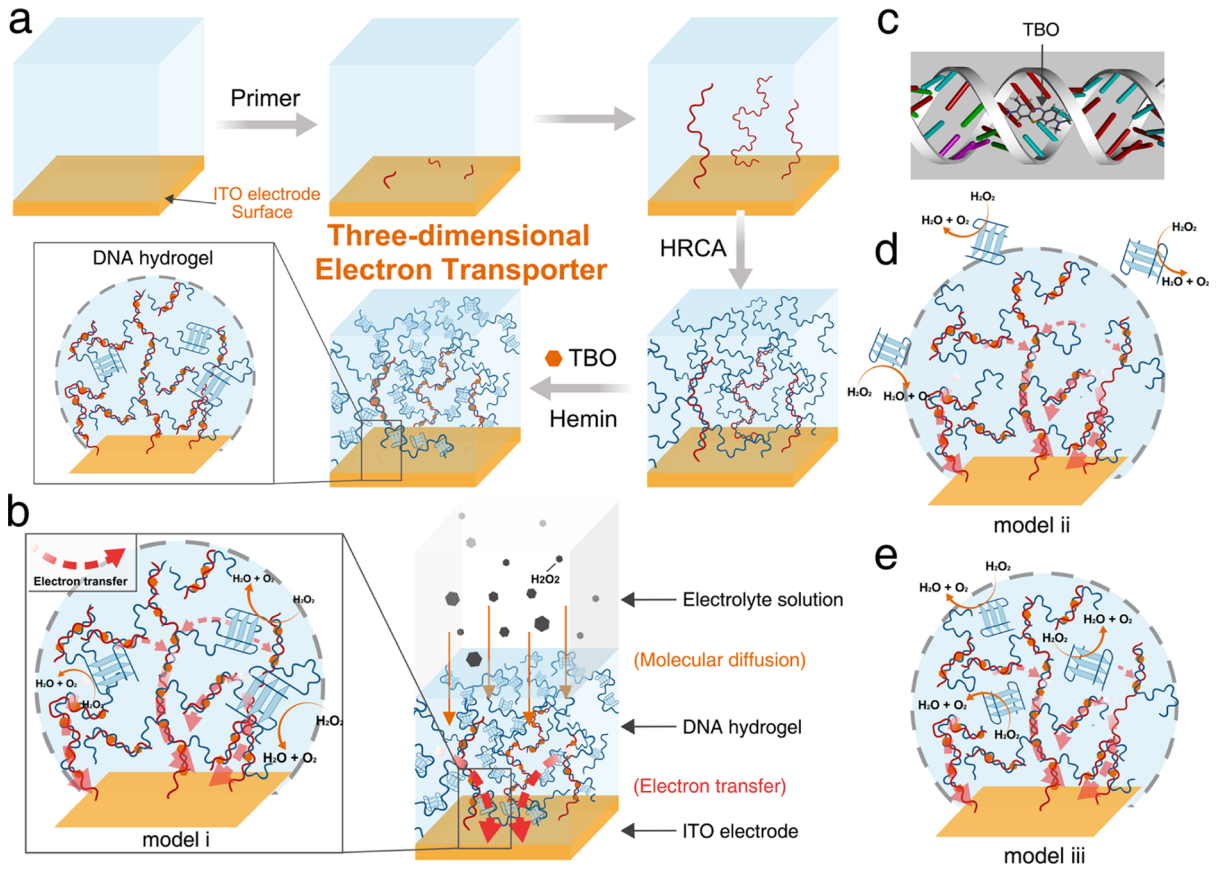

into the external solution of the DNA hydrogel and was allowed to incubate with the hydrogel for 2 h. Confocal laser scanning microscopy images of the DNA hydrogel were then obtained to study the diffusion of these substances. Three channels were adopted: green channel (fluorescent signal of SYBR Green I with an excitation wavelength of 488 nm and an emission wavelength of 505−550 nm), red channel (fluorescent signal of Cy3 with an excitation wavelength of 546 nm and an emission wavelength of 575−640 nm), and blue channel (fluorescent signal of DAPI with an excitation wavelength of 340 nm and an emission wavelength of 400−650 nm).

2.5. Fabrication of Control Models. Two other models were also fabricated to work as the control. In one of the models, the electron mediator TBO was intercalated in the hydrogel, while G-quadruplex/hemin DNAzyme was put in the electrolyte. In detail, the TBO-intercalated DNA hydrogel was prepared just as shown in section 2.2, using circular DNA 2 instead of circular DNA 1 and without the treatment of hemin. The prepared hydrogel contained no G-quadruplex/hemin DNAzyme. When performing electrochemical measurements, the ITO electrode functionalized with the TBO-intercalated DNA hydrogel was adopted as the working electrode. G-quadruplex/hemin DNAzyme (310 μM) alone was added in the electrolyte directly. The G-quadruplex/hemin DNAzyme alone was prepared by incubating 310 μM G-quadruplex with 20 μM hemin for 2 h in PBS solution.

In the other control model, the electron mediator TBO was intercalated in the hydrogel, while G-quadruplex/hemin DNAzyme was encapsulated in the hydrogel. In detail, the preparation of TBO-intercalated DNA hydrogel was similar to the above. The difference was that after the electrode was heated at 65 °C for 15 min to terminate the reaction and dissolve the DNA hydrogel, 310 μM G-quadruplex was added in the hydrogel and incubated at 4 °C for 1 h on a rotary shaker at a speed of 200 rpm. After being centrifuged at 4000 rpm at 4 °C for 5 min and washed twice, 20 μM hemin was added for 2 h incubation, and the DNAzyme-encapsulated DNA hydrogel was fabricated. Finally, the DNA hydrogel was incubated with 2 mM TBO for 1 h, followed by washing with PBS buffer to remove nonspecifically adsorbed TBO. Thereafter, the electrode was ready for electrochemical measurements. The control model was fabricated with 310 μM G-quadruplex/hemin DNAzyme, which was encapsulated in the DNA hydrogel instead of being incorporated at the node of the hydrogel scaffold like that in the three-dimensional electron transporter. The amount of the DNAzyme was verified the same as that of the three-dimensional electron transporter using colorimetric catalytic analysis (Figure S5).

2.6. Molecular Docking. Molecular docking of TBO and double-stranded DNA was performed by Discovery Studio 2018. The three-dimensional structure of TBO was obtained from ChemSpider, and the sequence of double-stranded DNA was the same as circular DNA 1. For molecular docking, the docking site and forcefield were imparted to double-stranded DNA first. Then, the best conformation of TBO was picked, and the forcefield was imparted. Finally, the double-stranded DNA was specified as the receptor, and TBO was docked to DNA.

https://dx.doi.org/10.1021/acsami.0c08064
ACS Appl. Mater. Interfaces 2020, 12, 36851−36859

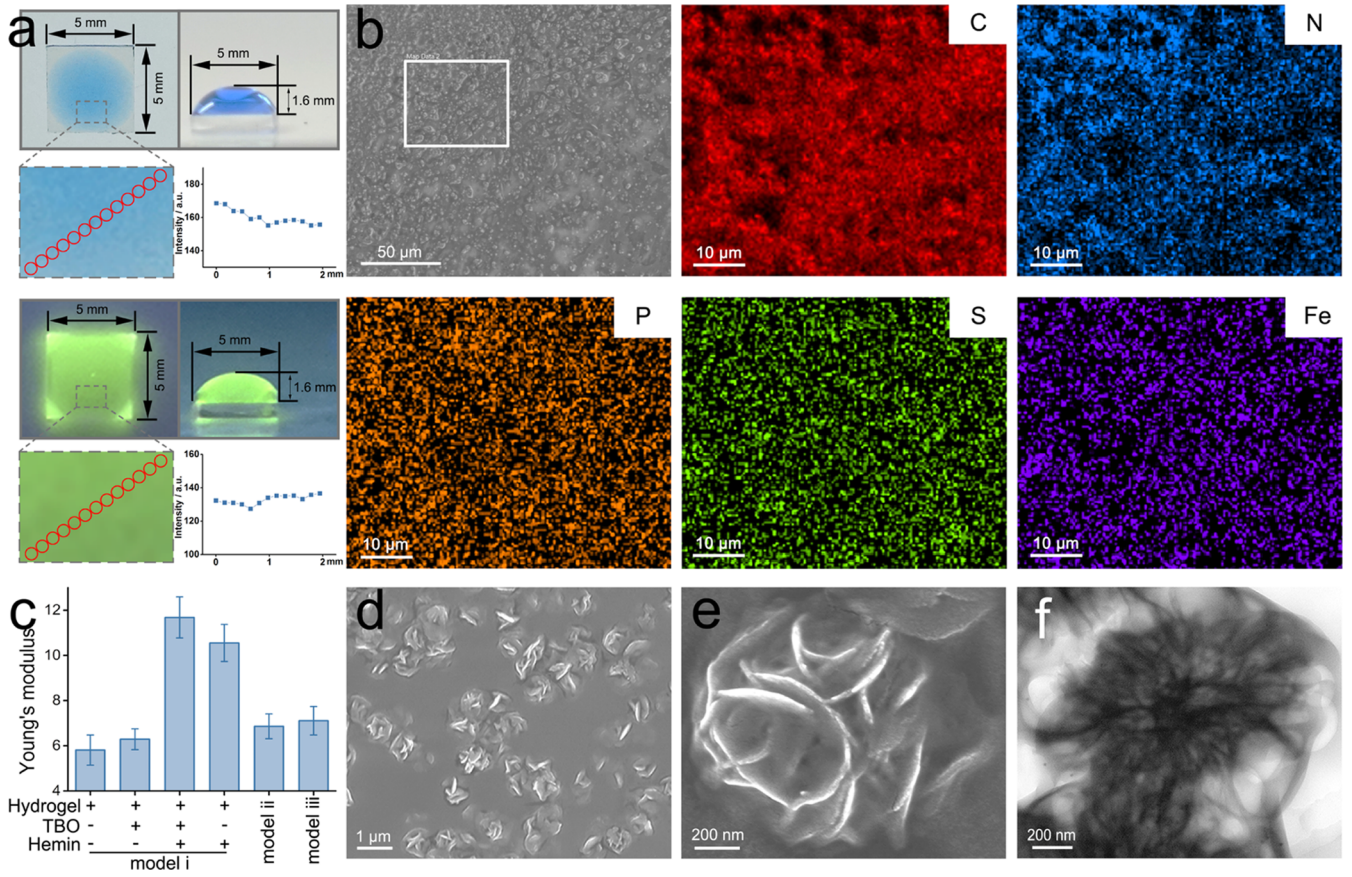

Figure 1. Characterization of the three-dimensional electron transporter. (a) Macroscopic observation of the TBO-intercalated (the upper part, snapped under sunlight) and SYBR Green I-stained (the lower part, snapped under UV lamp) DNA hydrogels. The color distribution was measured by ImageJ software. (b) SEM-EDS images of the distribution of C, N, P, S, and Fe in the TBO-intercalated and DNAzyme-incorporated DNA hydrogels (three-dimensional electron transporter). (c) Young's modulus of different DNA hydrogels. (d,e) SEM images of the three-dimensional electron transporter. (f) TEM image of the three-dimensional electron transporter.

3. RESULTS AND DISCUSSION

3.1. Principle of the DNA Hydrogel-Based Three-Dimensional Electron Transporter. The principle of the proposed DNA hydrogel-based three-dimensional electron transporter is shown in Scheme 1a,b. As illustrated, the product of HRCA is hyperbranched double-stranded DNA with a length of hundreds to thousands of base pairs. These networked long strands can serve as a scaffold to intercalate the electron mediator TBO, a phenothiazine dye which displays high binding affinity to duplex DNA through intercalative binding (Scheme 1c). Theoretically, TBO can be consecutively intercalated in the double-stranded DNA scaffold. Thus, electrons generated by a reaction far from the electrode surface can be eventually transported to and detected by the electrode through the mediation of TBO along the DNA scaffold. Here, to demonstrate the feasibility of the three-dimensional electron transporter, a well-established peroxidase-based electrochemical biosensing system is adopted, and three possible models are designed as follows: (i) G-quadruplex/hemin DNAzyme with intrinsic peroxidase-like activity is incorporated at the node of the hydrogel scaffold during the synthesis of the hydrogel because the G-quadruplex itself can be directly produced by HRCA (Scheme 1b). (ii) A separate DNAzyme is put in the electrolyte (Scheme 1d). (iii) The separate DNAzyme is encapsulated in the DNA hydrogel (Scheme 1e). The DNAzyme can generate electrons during the electrochemical catalysis of the reduction of H_2O_2.[28] Through the mediation of the DNA hydrogel-based three-dimensional electron transporter, acquisition of the electrochemical signal from long-distance electrochemical catalysis is expected to be achieved.

3.2. Characterization of the Electrode-Supported DNA Hydrogel. First, a macroscopic observation of the DNA hydrogel is performed. As shown in Figure 1a, TBO-intercalated hydrogel with a blue appearance can be clearly observed on the ITO electrode. The diameter and the height of the hydrogel are 5 and 1.6 mm, respectively. Here, the blue color originates from TBO. To further show the DNA scaffold, we use a conventional fluorescent DNA dye SYBR Green I (SGI) to label the DNA. In this case, the same shape of the DNA hydrogel with green fluorescence can be observed under UV light. By zooming in on the high-resolution image of the hydrogel and comparing the colors in different regions, we also found that the color distribution of both the TBO-intercalated hydrogel and SGI-labeled hydrogel is uniform, suggesting the even distribution of DNA and TBO in the hydrogel. The composition of the TBO-intercalated and DNAzyme-incorporated DNA hydrogel was measured by SEM-energy dispersive spectroscopy (SEM–EDS) elemental mapping (Figure 1b). Obviously, the distribution of C, N, P, S, and Fe has good uniformity. This result suggests the coexistence of DNA, TBO, and hemin in the hydrogel because P, S, and Fe are characteristic elements of DNA, TBO, and hemin, respectively.

https://dx.doi.org/10.1021/acsami.0c08064
ACS Appl. Mater. Interfaces 2020, 12, 36851−36859

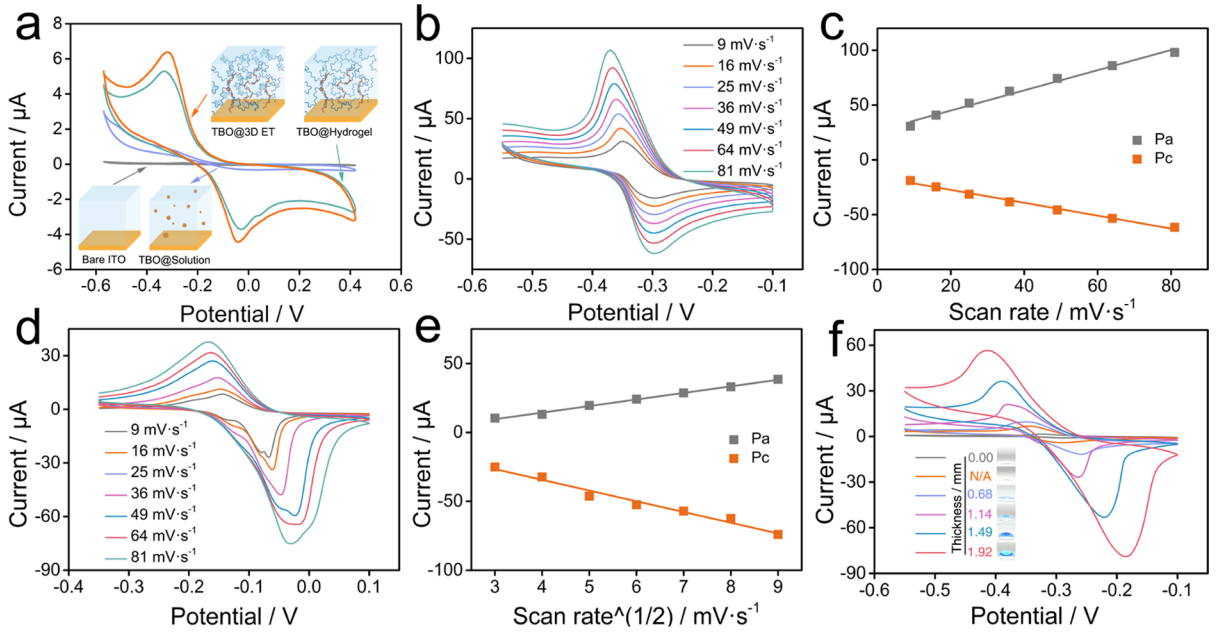

Figure 2. Verification of electron transport through the DNA hydrogel. (a) Schematic illustration and corresponding CV curves of bare ITO, TBO@Solution, and TBO@Hydrogel. 3D ET: three-dimensional electron transporter. (b) CV curves of TBO@Hydrogel at different scan rates (9−81 $mV·s^{-1}$) and (c) linear relationship between peak currents and scan rates. (d) CV curves of TBO@Solution at different scan rates (9−81 $mV·s^{-1}$) and (e) linear relationship between peak currents and square root of scan rates. (f) CV curves of TBO-intercalated DNA hydrogels with the same bottom area and different thicknesses. Pa and *Pc* represent the anodic peak and cathodic peak, respectively. The scan rate was 20 $mV·s^{-1}$.

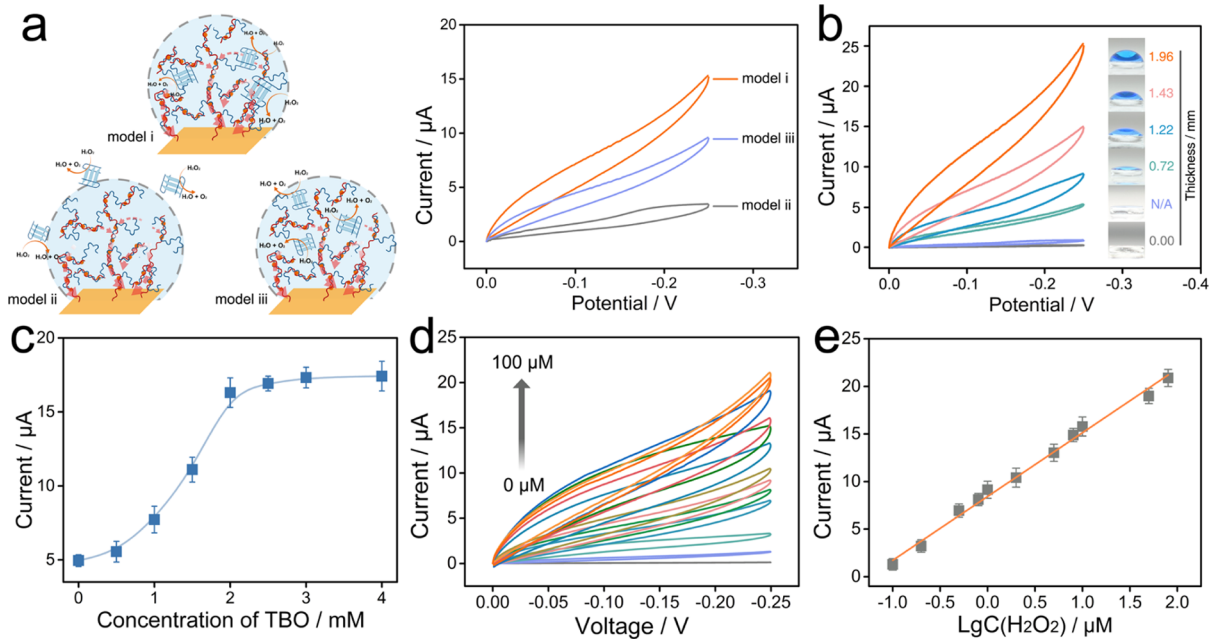

Figure 3. Application of the three-dimensional electron transporter for biosensing. (a) Schematic illustration and corresponding performance of different models in the detection of H_2O_2. (b) CV curves of the three-dimensional electron transporter with the same bottom area and different thicknesses in the detection of H_2O_2. (c) Optimization of the concentration of TBO in the fabrication of the three-dimensional electron transporter. (d) CV curves of the three-dimensional electron transporter in the detection of different concentrations of H_2O_2 in PBS solution. (e) Log-linear relationship between the peak current at −0.25 V and the logarithm of concentration of H_2O_2 in PBS solution. The scan rate was 20 $mV·s^{-1}$.

The Young's modulus of the DNA hydrogel was further measured. It is interesting that the DNA hydrogel either intercalated with TBO or not shows a Young's modulus around 6 kPa (6.29 ± 0.46 and 5.81 ± 0.67 kPa, respectively) (Figure 1c). However, while G-quadruplex/hemin DNAzyme is formed, the Young's modulus increases sharply to 11.68 ± 0.91 kPa. Experimental results of some control groups confirm that it is the incorporation of hemin that induces the increase of the Young's modulus (10.85 ± 0.82 kPa). Model (ii) and model (iii), in which G-quadruplex/hemin are separated in the electrolyte or hydrogel, show relatively lower Young's modulus (6.86 ± 0.55 and 7.11 ± 0.63 kPa, respectively), which is also

https://dx.doi.org/10.1021/acsami.0c08064
ACS Appl. Mater. Interfaces 2020, 12, 36851−36859

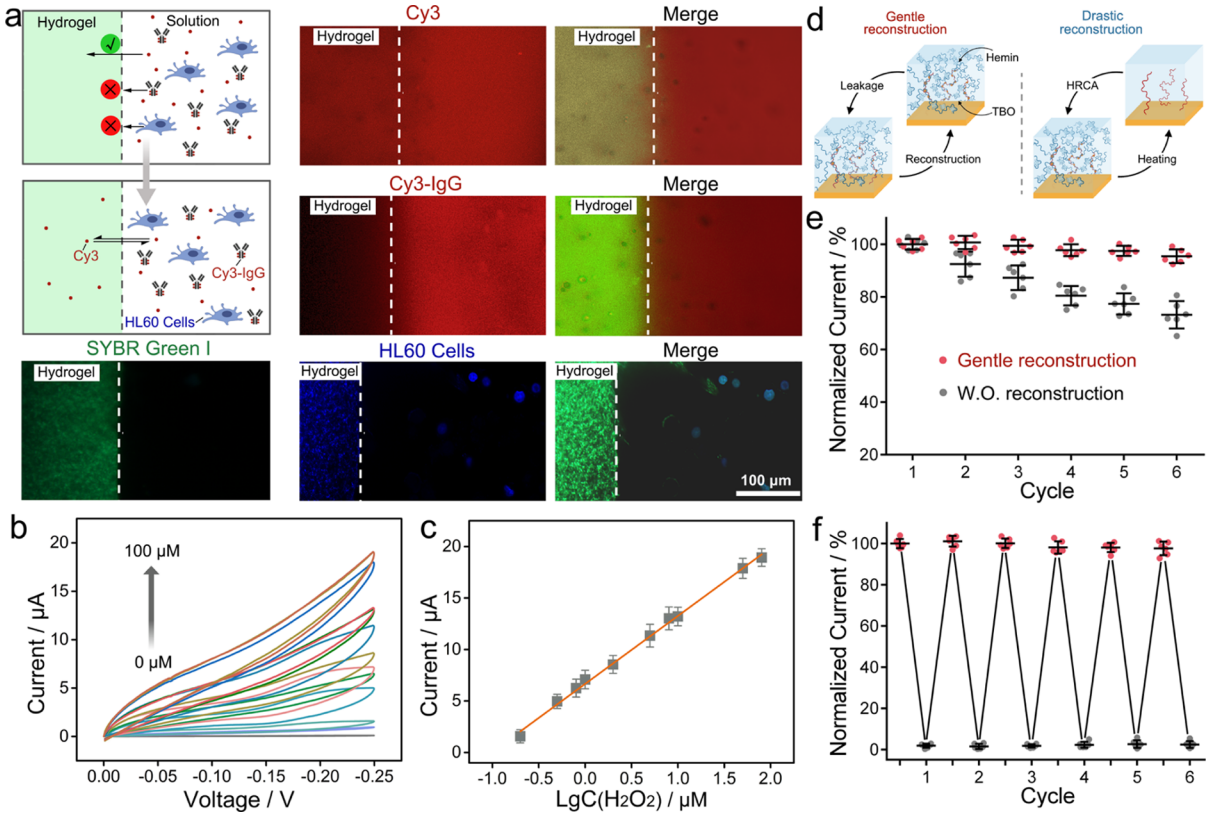

Figure 4. The anti-interference ability and reconstruction ability of the three-dimensional electron transporter. (a) Schematic illustration and confocal laser scanning microscopy images of the diffusion of micromolecules (Cy3), macromolecules (Cy3-IgG), and cells (HL60 cells prestained with DAPI) from solution to the DNA hydrogel. (b) CV curves of the three-dimensional electron transporter in the detection of different concentrations of H_2O_2 in 10% serum. (c) Log-linear relationship between the peak current at −0.25 V and the logarithm of concentration of H_2O_2. (d) Schematic illustration of gentle reconstruction and drastic reconstruction of the three-dimensional electron transporter. (e) Gentle reconstruction and (f) drastic reconstruction ability of the three-dimensional electron transporter. The scan rate was 20 $mV{\cdot}s^{-1}$.

consistent with the above results. The result is reasonable because hemin serves as a connection node among branched DNA strands, stabilizing the three-dimensional structure of the DNA hydrogel. The result is also favorable because the larger the Young's modulus, the less likely it is to deform and the more stable the structure. Finally, SEM and TEM were performed. As shown in Figure 1d,e, the surface of the dried DNA hydrogel shows nanoflower structures with a uniform size under SEM. The result coincides with some previous reports.[29,30] The TEM image shows a nanonetwork structure of the DNA hydrogel (Figure 1f).

3.3. Electron Transport through the DNA Hydrogel. Electron transport between the electron mediator TBO and the electrode through the DNA hydrogel was first studied using cyclic voltammetry. As shown in Figure 2a, a couple of well-defined redox peaks of TBO can be observed in the DNA hydrogel, regardless of the formation of the G-quadruplex. The anodic peak potential and cathodic peak potential are −0.30 V and −0.05 V, respectively. In contrast, when TBO is placed in the electrolyte in the absence of the DNA hydrogel, the redox peaks of TBO can still be observed, but the peak currents are greatly reduced, which is only about one-tenth of that in the DNA hydrogel. This result indicates that the DNA hydrogel greatly enhances the electron transport of TBO.

Further study on the relationship between peak currents and scan rates reveals that in the presence of the DNA hydrogel, the anodic and cathodic peaks currents are linear versus the scan rates in a range of 9−81 $mV{\cdot}s^{-1}$ (Figure 2b,c), which is characteristic of an adsorption-controlled electrochemical behavior.[31] Whereas for the TBO that is dissolved in the electrolyte, the peak currents are linear versus the square root of the scan rates in a range of 9−81 $mV{\cdot}s^{-1}$ (Figure 2d,e), suggesting a diffusion-controlled electrochemical behavior.[32] The differences in electrochemical behavior are in full agreement with the actual situation.

DNA hydrogels with the same bottom area and different thicknesses were also fabricated on the ITO electrode to study the long-distance electron transport. As shown in Figure 2f, there is a positive relationship between the peak currents and the thickness. Because the area of the electrode involved in electron transfer is the same, the increase in current should be attributed to the following factors: (1) long-distance electron transfer of the electroactive species in the DNA hydrogel that are not close to the electrode surface; (2) the increased effective electrode area arisen from the hydrogel which allows the electrolyte to enter and exit freely and becomes a part of the electrode; (3) increased mass transfer efficiency at the hydrogel−liquid interface instead of the solid−liquid interface. In addition, it is noted that a shift of *Pa* and *Pc* is also observed which should be caused by the increased resistance along with the long-distance electron transfer. The above results indicate the successful fabrication of the three-dimensional electron transporter with a considerable electron transfer effect and signal output intensity.

3.4. Application of the Three-Dimensional Electron Transporter for Biosensing. As shown in Figure 3a, three

https://dx.doi.org/10.1021/acsami.0c08064
ACS Appl. Mater. Interfaces 2020, 12, 36851−36859

models were studied for electrochemical biosensing. A detection range of −0.25 to 0 V, in which the catalytic peak of H_2O_2 is located, was selected for the detection of H_2O_2.[27] In the case of model (i), a significant electrocatalytic current is observed toward the reduction of H_2O_2. In contrast, in the case of model (ii) and (iii), the current response is greatly reduced. For model (ii), the electron transfer relies on the diffusion of the DNAzyme to the surface of the DNA hydrogel, which greatly limits the electrocatalysis. For model (iii), although the DNAzyme is also located in the hydrogel just like model (i), there is a relative large distance between the DNAzyme and the electron mediator due to simple physical encapsulation, leading to lower encapsulation efficiency of DNAzyme and the decrease of the efficiency of the electrochemical catalysis. The above results show that the regular incorporation of electroactive molecular elements (herein DNAzyme) in the DNA hydrogel can maximize the role of the three-dimensional electron transporter, thereby laying the foundation for high-performance biosensing. Model (i), that is, the ITO electrode functionalized with the TBO-intercalated and DNAzyme-incorporated DNA hydrogels, was then adopted for the following study because it has the best performance. DNA hydrogels with different thicknesses were fabricated to study the biosensing performance.

As shown in Figure 3b, the electrocatalytic current increases with the thickness, suggesting that the DNAzyme that is relatively far from the electrode can still be involved in the electrocatalysis through the mediation of the three-dimensional electron transporter. TBO with different amounts was also applied. As shown in Figure 3c, a sigmoidal curve of the catalytic current versus the TBO concentration can be observed with a sharp inflection point at 1.5 mM. This phenomenon that the electrocatalytic signal jumps sharply near the inflection point instead of continuously changing with the TBO concentration can be elucidated as follows: because the three-dimensional electron transfer relies on the mediation of TBO assembled on the DNA scaffold in an orderly manner, lower TBO concentration may lead to the loss of TBO at some sites on the DNA scaffold, which will cause the electrons to fail to pass through the DNA strand to the electrode. Detection of H_2O_2 was then performed. As shown in Figure 3d,e, the electrocatalytic currents rise along with the increased concentration of H_2O_2. A linear relationship is obtained between the currents at −0.25 V and the logarithm of H_2O_2 concentrations. The regression equation is $y = 6.706x + 8.428$, where x stands for the logarithm of the H_2O_2 concentration, and y is the electrocatalytic current. The detection range is from 0.1 to 80 μM, and the detection limit is 0.07 μM ($3\sigma/k$, σ: the standard deviation of the blank sample, k: the slope of the linear regression curve, and correlation coefficient = 0.997). Compared to some previously reported biosensors for the detection of H_2O_2,[33−36] our strategy based on the three-dimensional electron transporter exhibits superior performance with the detection limit increased dozens of times (Table S1). Besides, the sensitivity of the three-dimensional electron transporter is superior to some existing electrochemical biosensors in the detection of H_2O_2 (Table S1).

3.5. Anti-interference and Reconstruction of the Three-Dimensional Electron Transporter. Before conducting biosensing in real samples, for example, the serum sample for diagnostic purposes, the anti-interference capability of the three-dimensional electron transporter was studied. Diffusion of Cy3 (a micromolecular fluorophore), Cy3-labeled IgG (a fluorophore-labeled macromolecular protein), and the HL60 cell (a human caucasian promyelocytic leukemia cell, whose nucleus was stained with DAPI) from external solution into the three-dimensional electron transporter was measured. As shown in Figure 4a, only micromolecules can freely diffuse into the three-dimensional electron transporter, while macromolecules and cells are excluded. In this way, the three-dimensional electron transporter can be used as a molecular sieve, facilitating the fabrication of a biosensor for the detection of micromolecular substances in complex samples. Here, detection of H_2O_2 in the serum sample is achieved (Figure 4b,c). The detection range is from 0.2 to 80 μM, similar with that in PBS. The detection limit is 0.15 μM ($3\sigma/k$, σ: the standard deviation of the blank sample, k: the slope of the linear regression curve, and correlation coefficient = 0.998).

Reconstruction of the three-dimensional electron transporter was conducted in two different ways: a gentle way and a drastic way (Figure 4d). For the former, after electrochemical measurement, the electrode functionalized with the three-dimensional electron transporter was taken from the electrolyte and placed in PBS containing 2 mM TBO and 20 μM hemin for 2 h to replenish TBO and hemin that may be lost. Afterward, the electrode was ready for another measurement. For the latter, the electrode was heated at 70 °C for 15 min to remove all the substances except the LRCA product that is attached to the electrode through the covalent bond. Thereafter, the electrode was reconstructed following the protocol of the fabrication of the DNA hydrogel-based three-dimensional electron transporter. Both ways are shown to be effective (Figure 4e,f). In detail, the electrochemical signal keeps steady in a gentle reconstruction group, as shown in Figure 4e, indicating that the DNA scaffold of the three-dimensional electron transporter has good stability. In contrast, signal loss is observed without reconstruction (W.O. reconstruction group), which should be attributed to the leakage of TBO and hemin during the detection cycle. As for drastic reconstruction, even after six "heating depolymerization−HRCA polymerization" cycles, the electrochemical signal remains unchanged (Figure 4f), which demonstrates that this three-dimensional electron transporter has superior reproducibility. So, the electrode can be reconstructed and applied for multiple measurements.

In comparison with some other three-dimensional DNA scaffold, for example, the hybrid DNA hydrogel and DNA origami, the DNA hydrogel used here has some advantages in the construction of the three-dimensional electron transporter: (i) the DNA hydrogel used here has macroscopic three-dimensional networks and huge swelling capacity, which are suitable to entrap bioactive molecules to be applied in liquid−solid interfacial biosensing. (ii) The pure DNA hydrogel has potential universality. According to our previous research studies,[26,27] a pure DNA hydrogel can be used as the scaffold material to encapsulate natural enzymes or nanozymes and maintain their biological activities. (iii) The DNA hydrogel has the ability to be reconstructed for bioanalysis.

4. CONCLUSIONS

In summary, we have successfully fabricated a three-dimensional electron transporter on a conventional working electrode by using the electrode-supported DNA hydrogel as a networked scaffold. TBO, a kind of electron mediator, is intercalated in the DNA scaffold with a regular arrangement to

https://dx.doi.org/10.1021/acsami.0c08064
ACS Appl. Mater. Interfaces 2020, 12, 36851−36859

transfer long-distance electrons to the electrode surface through electron hopping. In comparison with conventional unfunctionalized electrodes, better electron transfer effect and signal output intensity can be achieved by using the three-dimensional electron transporter. Further incorporation of electroactive molecular elements (herein DNAzyme) into the DNA hydrogel endows the three-dimensional electron transporter with biosensing functions. Detection of H_2O_2 as a model is thereby achieved with an outstanding performance. The proposal and successful implementation of the concept of the three-dimensional electron transporter makes it possible to break through the limitations of two-dimensional electrodes, providing potential support for the development of high-performance biosensors.

■ ASSOCIATED CONTENT

Supporting Information

The Supporting Information is available free of charge at https://pubs.acs.org/doi/10.1021/acsami.0c08064.

Optimization of amplification time of LRCA; optimization of the concentration of hemin; optimization of the incubation time of hemin; dependence of the electrochemical performance on the pH; optimization of the concentration of the G-quadruplex used in the fabrication of the DNAzyme-encapsulated DNA hydrogel; and comparison of the detection performance of this work with some other methods (PDF)

■ AUTHOR INFORMATION

Corresponding Authors

Farid A. Harraz − *Promising Centre for Sensors and Electronic Devices (PCSED), Advanced Materials and Nano-Research Centre, Najran University, Najran 11001, Saudi Arabia; Nanomaterials and Nanotechnology Department, Central Metallurgical Research and Development Institute (CMRDI), Helwan, Cairo 11421, Egypt*; Email: faharraz@nu.edu.sa

Xiaoli Zhu − *Center for Molecular Recognition and Biosensing, School of Life Sciences, Shanghai University, Shanghai 200444, China*; orcid.org/0000-0001-5497-4538; Email: xiaolizhu@shu.edu.cn

Authors

Xiaoxia Mao − *Center for Molecular Recognition and Biosensing, School of Life Sciences, Shanghai University, Shanghai 200444, China; Key Laboratory of Aqueous Environment Protection and Pollution Control of Yangtze River in Anhui of Anhui Provincial Education Department, College of Resources and Environment, Anqing Normal University, Anqing 246011, China*

Dongsheng Mao − *Center for Molecular Recognition and Biosensing, School of Life Sciences, Shanghai University, Shanghai 200444, China*

Tianshu Chen − *Center for Molecular Recognition and Biosensing, School of Life Sciences, Shanghai University, Shanghai 200444, China*

Mohammed Jalalah − *Promising Centre for Sensors and Electronic Devices (PCSED), Advanced Materials and Nano-Research Centre, Najran University, Najran 11001, Saudi Arabia*

Mohammed S. Al-Assiri − *Promising Centre for Sensors and Electronic Devices (PCSED), Advanced Materials and Nano-Research Centre, Najran University, Najran 11001, Saudi Arabia*

Genxi Li − *Center for Molecular Recognition and Biosensing, School of Life Sciences, Shanghai University, Shanghai 200444, China; State Key Laboratory of Pharmaceutical Biotechnology, Collaborative Innovation Center of Chemistry for Life Sciences, Department of Biochemistry, Nanjing University, Nanjing 210093, China*

Complete contact information is available at: https://pubs.acs.org/10.1021/acsami.0c08064

Author Contributions

X.M. and D.M. contributed equally in this work. X.Z. designed this work; X.M. and D.M. fabricated the DNA hydrogel. X.M. carried out electrochemical measurements. T.C. conducted characterizations of the hydrogel. G.L. fabricated the control models. M.J. and M.S.A.-A. performed anti-interference experiment and molecular docking. F.A.H. analyzed the results. X.Z., X.M., and D.M. wrote and edited the manuscript.

Notes

The authors declare no competing financial interest.

■ ACKNOWLEDGMENTS

This work was supported by the National Natural Science Foundation of China (Grant numbers 21575088 and 31800670) and the Natural Science Foundation of Shanghai (Grant number 19ZR1474200). Authors would also like to acknowledge the support of the Ministry of Education, Kingdom of Saudi Arabia, for this research by a grant (PCSED-003-18) under the Promising Centre for Sensors and Electronic Devices (PCSED) at Najran University, Kingdom of Saudi Arabia.

■ REFERENCES

(1) Song, P.; Shen, J.; Ye, D.; Dong, B.; Wang, F.; Pei, H.; Wang, J.; Shi, J.; Wang, L.; Xue, W.; Huang, Y.; Huang, G.; Zuo, X.; Fan, C. Programming Bulk Enzyme Heterojunctions for Biosensor Development with Tetrahedral DNA Framework. *Nat. Commun.* **2020**, *11*, 838.

(2) Metzger, T. S.; Chandaluri, C. G.; Tel-Vered, R.; Shenhar, R.; Willner, I. Donor/Acceptor-Modified Electrodes for Photoelectrochemical and Photobioelectrochemical Applications. *Adv. Funct. Mater.* **2016**, *26*, 7148−7155.

(3) Drummond, T. G.; Hill, M. G.; Barton, J. K. Electrochemical DNA Sensors. *Nat. Biotechnol.* **2003**, *21*, 1192−1199.

(4) Labib, M.; Sargent, E. H.; Kelley, S. O. Electrochemical Methods for the Analysis of Clinically Relevant Biomolecules. *Chem. Rev.* **2016**, *116*, 9001−9090.

(5) Felix, F. S.; Angnes, L. Electrochemical Immunosensors - A Powerful Tool for Analytical Applications. *Biosens. Bioelectron.* **2018**, *102*, 470−478.

(6) Shin, H.; Sharma, B. K.; Lee, S. W.; Lee, J.-B.; Choi, M.; Hu, L.; Park, C.; Choi, J. H.; Kim, T. W.; Ahn, J.-H. Stretchable Electroluminescent Display Enabled by Graphene-Based Hybrid Electrode. *ACS Appl. Mater. Interfaces* **2019**, *11*, 14222−14228.

(7) Tyagi, D.; Wang, H.; Huang, W.; Hu, L.; Tang, Y.; Guo, Z.; Ouyang, Z.; Zhang, H. Recent Advances in Two-Dimensional-Material-Based Sensing Technology Toward Health and Environmental Monitoring Applications. *Nanoscale* **2020**, *12*, 3535−3559.

(8) Cao, L.; Xu, L.; Zhao, D.; Tahara, K.; Tobe, Y.; De Feyter, S.; Lei, S. Efficient Molecular Recognition Based on Nonspecific Van Der Waals Interaction at the Solid/Liquid Interface. *Chem. Commun.* **2014**, *50*, 11946−11949.

(9) Wang, Y.; Ning, G.; Wu, Y.; Wu, S.; Zeng, B.; Liu, G.; He, X.; Wang, K. Facile Combination of Beta-Cyclodextrin Host-Guest Recognition with Exonuclease-Assistant Signal Amplification for

Sensitive Electrochemical Assay of Ochratoxin A. *Biosens. Bioelectron.* **2019**, *124*−*125*, 82−88.
(10) An, Y.; Jin, T.; Zhu, Y.; Zhang, F.; He, P. An Ultrasensitive Electrochemical Aptasensor for the Determination of Tumor Exosomes Based on Click Chemistry. *Biosens. Bioelectron.* **2019**, *142*, 111503.
(11) Kelch, J.; Delaney, A.; Kelleher, F.; Baker, P.; Iwuoha, E.; Dempsey, E. Impedimetric and Electrochemical Evaluation of a New Redox Active Steroid Derivative for Hormone Immunosensing. *Biosens. Bioelectron.* **2020**, *150*, 111876.
(12) de Lima, L. F.; Pereira, E. A.; Ferreira, M. Electrochemical Sensor for Propylparaben Using Hybrid Layer-by-Layer Films Composed of Gold Nanoparticles, Poly(Ethylene Imine) and Nickel(II) Phthalocyanine Tetrasulfonate. *Sens. Actuators, B* **2020**, *310*, 127893.
(13) Sharma, N.; Panneer Selvam, S.; Yun, K. Electrochemical Detection of Amikacin Sulphate Using Reduced Graphene Oxide and Silver Nanoparticles Nanocomposite. *Appl. Surf. Sci.* **2020**, *512*, 145742.
(14) Zhu, M.; Chen, J.; Huang, L.; Ye, R.; Xu, J.; Han, Y. F. Covalently Grafting Cobalt Porphyrin onto Carbon Nanotubes for Efficient CO 2 Electroreduction. *Angew. Chem., Int. Ed.* **2019**, *58*, 6595−6599.
(15) Jiang, B.; Li, C.; Qian, H.; Hossain, M. S. A.; Malgras, V.; Yamauchi, Y. Layer-by-Layer Motif Architectures: Programmed Electrochemical Syntheses of Multilayer Mesoporous Metallic Films with Uniformly Sized Pores. *Angew. Chem., Int. Ed.* **2017**, *56*, 7836−7841.
(16) Wang, L.; Xiong, Q.; Xiao, F.; Duan, H. 2D Nanomaterials Based Electrochemical Biosensors for Cancer Diagnosis. *Biosens. Bioelectron.* **2017**, *89*, 136−151.
(17) Zhang, M.-Y.; Song, Y.; Guo, D.; Yang, D.; Sun, X.; Liu, X.-X. Strongly Coupled Polypyrrole/Molybdenum Oxide Hybrid Films via Electrochemical Layer-by-Layer Assembly for Pseudocapacitors. *J. Mater. Chem. A* **2019**, *7*, 9815−9821.
(18) Li, J.; Mo, L.; Lu, C.-H.; Fu, T.; Yang, H.-H.; Tan, W. Functional Nucleic Acid-Based Hydrogels for Bioanalytical and Biomedical Applications. *Chem. Soc. Rev.* **2016**, *45*, 1410−1431.
(19) Li, Y.; Ma, Y.; Jiao, X.; Li, T.; Lv, Z.; Yang, C. J.; Zhang, X.; Wen, Y. Control of Capillary Behavior Through Target-Responsive Hydrogel Permeability Alteration for Sensitive Visual Quantitative Detection. *Nat. Commun.* **2019**, *10*, 1036.
(20) Chang, Y.; Li, M.; Wu, Z.; Zhuo, Y.; Chai, Y.; Xiao, Q.; Yuan, R. Homogeneous Entropy Catalytic-Driven DNA Hydrogel as Strong Signal Blocker for Highly Sensitive Electrochemical Detection of Platelet-Derived Growth Factor. *Anal. Chem.* **2018**, *90*, 8241−8247.
(21) Wang, C.; Li, F.; Bi, Y.; Guo, W. Reversible Modulation of 2D Photonic Crystals with a Responsive Shape-Memory DNA Hydrogel Film. *Adv. Mater. Interfaces* **2019**, *6*, 1900556.
(22) Guo, B.; Wen, B.; Cheng, W.; Zhou, X.; Duan, X.; Zhao, M.; Xia, Q.; Ding, S. An Enzyme-Free and Label-Free Surface Plasmon Resonance Biosensor for Ultrasensitive Detection of Fusion Gene Based on DNA Self-Assembly Hydrogel with Streptavidin Encapsulation. *Biosens. Bioelectron.* **2018**, *112*, 120−126.
(23) Chen, F.; Xue, J.; Zhang, J.; Bai, M.; Yu, X.; Fan, C.; Zhao, Y. Differentiated Visualization of Single-Cell 5-Hydroxymethylpyrimidines with Microfluidic Hydrogel Encoding. *J. Am. Chem. Soc.* **2020**, *142*, 2889−2896.
(24) Gacanin, J.; Synatschke, C. V.; Weil, T. Biomedical Applications of DNA-Based Hydrogels. *Adv. Funct. Mater.* **2020**, *30*, 1906253.
(25) Zhu, X.; Gao, L.; Tang, L.; Peng, B.; Huang, H.; Wang, J.; Yu, J.; Ouyang, X.; Tan, J. Ultrathin PtNi Nanozyme Based Self-Powered Photoelectrochemical Aptasensor for Ultrasensitive Chloramphenicol Detection. *Biosens. Bioelectron.* **2019**, *146*, 111756.
(26) Zhu, X.; Mao, X.; Wang, Z.; Feng, C.; Chen, G.; Li, G. Fabrication of Nanozyme@DNA Hydrogel and Its Application in Biomedical Analysis. *Nano Res.* **2017**, *10*, 959−970.
(27) Mao, X.; Chen, G.; Wang, Z.; Zhang, Y.; Zhu, X.; Li, G. Surface-Immobilized and Self-Shaped DNA Hydrogels and Their Application in Biosensing. *Chem. Sci.* **2018**, *9*, 811−818.
(28) Travascio, P.; Li, Y.; Sen, D. DNA-Enhanced Peroxidase Activity of a DNA Aptamer-Hemin Complex. *Chem. Biol.* **1998**, *5*, 505−517.
(29) Huang, Y.; Xu, W.; Liu, G.; Tian, L. Pure DNA Hydrogel with Stable Catalytic Ability Produced by One-Step Rolling Circle Amplification. *Chem. Commun.* **2017**, *53*, 3038−3041.
(30) Mao, X.; Pan, S.; Zhou, D.; He, X.; Zhang, Y. Fabrication of DNAzyme-Functionalized Hydrogel and Its Application for Visible Detection of Circulating Tumor DNA. *Sens. Actuators, B* **2019**, *285*, 385−390.
(31) Murray, R. W. *Chemically Modified Electrodes*; Marcel Dekker: New York, 1984.
(32) Chen, X. R.; Yao, Y. X.; Yan, C.; Zhang, R.; Cheng, X. B.; Zhang, Q. A Diffusion-Reaction Competition Mechanism to Tailor Lithium Deposition for Lithium-Metal Batteries. *Angew. Chem., Int. Ed.* **2020**, *59*, 7743.
(33) Zhou, Z.; Yang, L.; Huang, L.; Liao, Y.; Liu, Y.; Xiao, Q. A Novel Fluorescent Probe for H_2O_2 Detection Based on CdSe@ZnS Quantum Dots/Ag Nanocluster Hybrid. *Anal. Chim. Acta* **2020**, *1106*, 176−182.
(34) Yeh, M.-H.; Li, Y.-S.; Chen, G.-L.; Lin, L.-Y.; Li, T.-J.; Chuang, H.-M.; Hsieh, C.-Y.; Lo, S.-C.; Chiang, W.-H.; Ho, K.-C. Facile Synthesis of Boron-Doped Graphene Nanosheets with Hierarchical Microstructure at Atmosphere Pressure for Metal-Free Electrochemical Detection of Hydrogen Peroxide. *Electrochim. Acta* **2015**, *172*, 52−60.
(35) Mattarozzi, L.; Cattarin, S.; Comisso, N.; Guerriero, P.; Musiani, M.; Verlato, E. Preparation of Porous Nanostructured Ag Electrodes for Sensitive Electrochemical Detection of Hydrogen Peroxide. *Electrochim. Acta* **2016**, *198*, 296−303.
(36) Zhao, K.; Gu, W.; Zheng, S.; Zhang, C.; Xian, Y. SDS-MoS_2 Nanoparticles as Highly-Efficient Peroxidase Mimetics for Colorimetric Detection of H_2O_2 and Glucose. *Talanta* **2015**, *141*, 47−52.

https://dx.doi.org/10.1021/acsami.0c08064
ACS Appl. Mater. Interfaces 2020, 12, 36851−36859